Sequential Symmetry-Breaking Events as a Synthetic Pathway for Chiral Gold Nanostructures with Spiral Geometries

Spencer D. Golze, Stefania Porcu, Chen Zhu, Eli Sutter, Pier Carlo Ricci, Edward C. Kinzel, Robert A. Hughes, and Svetlana Neretina*

Read Online

ACCESS | 📊 Metrics & More | 📄 Article Recommendations | 🆂🅸 Supporting Information

ABSTRACT: Symmetry-breaking synthetic controls allow for nanostructure geometries that are counter to the underlying crystal symmetry of a material. If suitably applied, such controls provide the means to drive an isotropic metal along a growth pathway yielding a three-dimensional chiral geometry. Herein, we present a light-driven solution-based synthesis yielding helical gold spirals from substrate-bound seeds. The devised growth mode relies on three separate symmetry-breaking events ushered in by seeds lined with planar defects, a capping agent that severely frustrates early stage growth, and the Coulombic repulsion that occurs when identically charged growth fronts collide. Together they combine to advance a growth pathway in which planar growth emanates from one side of the seed, advances to encircle the seed from both clockwise and counterclockwise directions, and then, upon collision of the two growth fronts, sees one front rise above the other to realize a self-perpetuating three-dimensional spiral structure.

KEYWORDS: chiral, plasmonics, gold, helix, spiral, symmetry-breaking
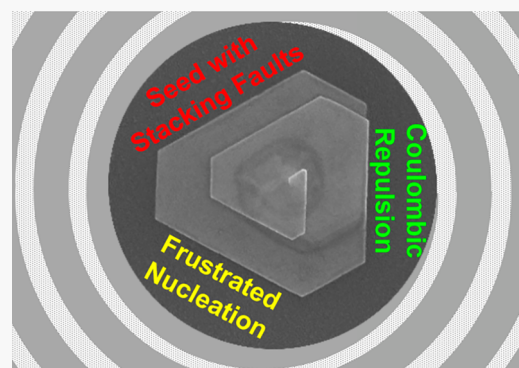
With remarkable light-manipulating capabilities and a chemistry that is woven into the fabric of life, chiral materials represent a topic of fundamental importance. As an intrinsically shape-dependent property that is accessible on all length scales, chirality has predictably become the focus of a broad effort directed toward the synthesis and fabrication of chiral nanostructures from otherwise achiral bulk materials.[1−4] Within this realm, it is the union of plasmonic and chiroptical responses that present some of the most intriguing opportunities.[5−10] Indeed, plasmonic materials with chiral configurations have not only emulated the optical properties of their molecular counterparts but have done so with a chiroptical activity that is as much as 10 orders of magnitude greater.[5] As such, it has spawned the field of chiral plasmonics with a host of applications ranging from biosensing[11−13] to metamaterials[10] to chiral photochemistry.[14,15]

Of all the techniques used to produce chiral plasmonic materials, it is those that are reliant on lithographic procedures that have resulted in the highest level of control over nanostructure shape, positioning, and enantiomer selection. Although such capabilities are unrivaled, these top-down approaches are disadvantageous from the standpoints that they are highly sophisticated, cost-prohibitive, and reliant on time-consuming serial processes and are often limited to planar geometries. Three-dimensional chiral geometries, which can express superior chiroptical activity, have been produced using more advanced lithographic techniques[16−18] but where the associated technological barriers limit their widespread use. Other approaches responsive to the drawbacks of conventional lithographic techniques have resorted to the use of glancing-angle depositions[19−21] and colloidal lithography.[22]

An alternate approach for preparing chiral plasmonic structures exploits the exacting chemical controls accessible through colloidal chemistry. With Au being one of the most desirable plasmonic metals, it becomes a daunting synthetic challenge to impose a chiral character upon a growing nanostructure because the asymmetries of such a morphology are in stark contradiction to the underlying symmetries of its fcc crystal structure. In many instances, this formidable challenge has been circumvented through the placement of achiral nanostructures on chiral templates[23] or through their assembly into chiral patterns using techniques such as peptide-based assembly[24] and DNA origami.[25] Notwithstanding, synthetic protocols have been devised that realize colloidal Au nanostructures that are intrinsically chiral.[26−34] Among these, the protocol of Nam and co-workers[26] stands out because they were able to devise an enantiomer-selective
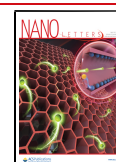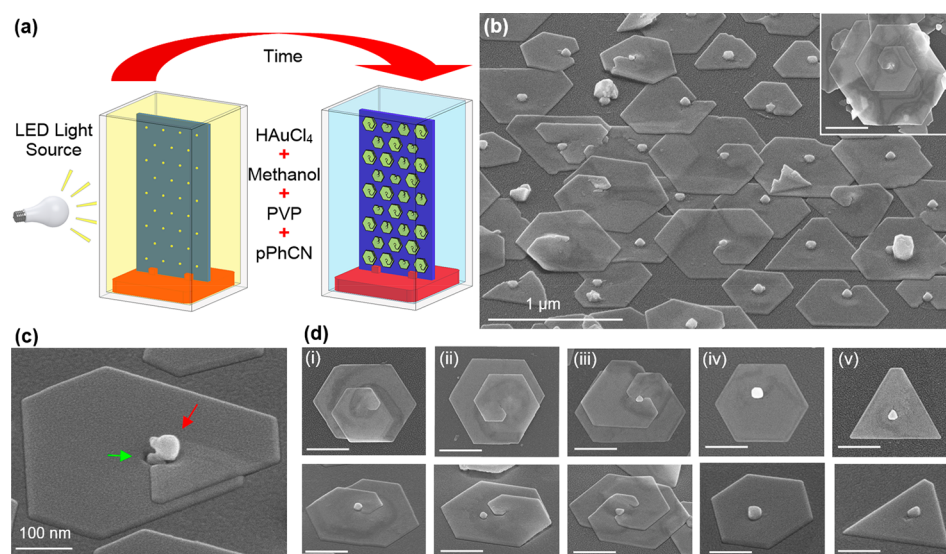
Figure 1. (a) Schematic representation of the experimental setup used to synthesize substrate-based chiral nanostructures via a plasmon-mediated growth mode. SEM images showing (b) the structures that emerge after a 4 h synthesis, (c) a high-magnification view at a seed location that initiated a spiral growth mode, and (d) the five most commonly observed structures with a plate-like morphology. The scale bar for all insets is 200 nm.
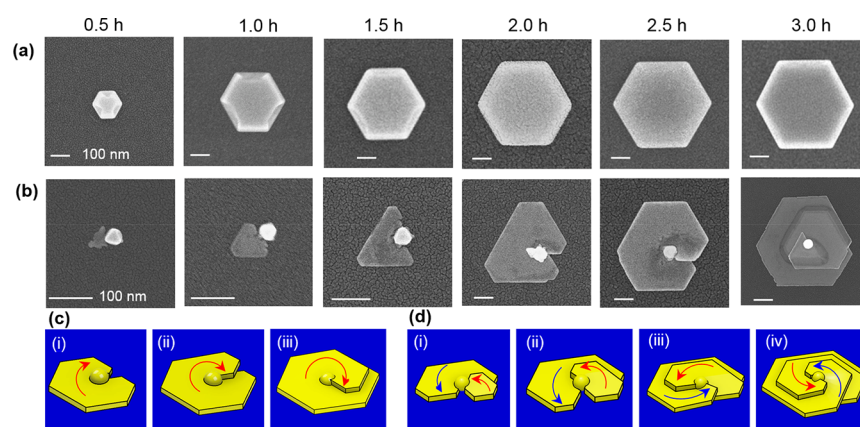

Figure 2. Time sequence showing the growth progressions observed for a (a) hexagonal Au nanoplate grown in $HAuCl_4$, PVP, methanol, and H_2O and (b) Au spiral grown in an identical solution to which pPhCN is added. Schematics showing the growth of a (c) single spiral and (d) the inferred growth mode for a double spiral.

synthesis where the six faces of a cube-like structure developed surface contours with a chiral character whose handedness depends on the handedness of the surface ligand applied. Other protocols have advanced synthetic procedures that transform what is nominally a planar growth mode into one that realizes a helical spiral.[27−31] Even though yields are low and the understanding of these growth modes is far from complete, the emergence of a quintessential three-dimensional chiral structure in a liquid-phase chemical environment is one that invokes both fascination and inquiry.

Recently, we devised a processing route for defining periodic arrays of substrate-based Au seeds lined with planar defects.[35] The break in symmetry afforded by these defects allowed for the demonstration of a light-mediated solution-based synthesis yielding arrays of Au nanoplates. Herein, it is demonstrated that through the application of additional synthetic controls, it is possible to break the symmetry of this planar growth mode so as to realize helical spirals. The spiral synthesis, while amenable to a one-pot strategy, is prone to significantly higher yields when it capitalizes on the ability to rapidly transfer the

sample from one growth solution to another where each chemical environment is designed to efficiently redirect the growth toward a particular symmetry-breaking event. The resulting growth mode is unique in that a chiral growth trajectory is facilitated by planar growth fronts that pivot around a centrally located seed, and as a result, eliminates the need for a screw dislocation.

Chiral Au nanostructures were produced using a synthetic strategy in which substrate-immobilized seeds are subjected to a liquid-phase chemical environment promoting a spiral geometry. The seeds were fabricated using benchtop processing routes in which either nanoimprint lithography or microsphere photolithography is used to define a periodic array of disc-like structures that, when heated, assemble into near-hemispherical Au nanostructures.[35−37] The majority of seeds produced in this manner are [111]-oriented single crystals with planar stacking faults that run parallel to the substrate surface.[35] Such defects are crucial to the synthesis of Au nanoplates because they provide an otherwise isotropic metal with a symmetry-breaking structure having a two-

dimensional character.[38,39] The spiral growth solution is an aqueous mixture of $HAuCl_4$, PVP, methanol, and protonated phenyl-modified carbon nitride (pPhCN). The synthesis proceeds via a plasmon-mediated growth mode in which LSPR-generated hot electron−hole pairs drive the reaction. The synthesis is adapted from a substrate-based nanoplate growth mode[35,40] whose mechanistic framework was detailed by Wei and co-workers.[40] It sees Au^{3+} ions reduced onto the seed by the excited electrons as the excited holes are scavenged by methanol. The reduction process is, however, reliant on PVP because it extends the hot electron lifetime to values commensurate with the time interval needed for the reaction to occur. Because PVP selectively binds to the planar defects at the perimeter of a nanostructure, a two-dimensional nanoplate evolves. With the only difference between this nanoplate synthesis and the spiral synthesis being the inclusion of pPhCN,[41,42] it is evident that this polymer plays a vital role.

Figure 1 summarizes the results obtained from a 4 h plasmon-mediated synthesis during which 60 nm Au seeds were immersed in the aforementioned spiral growth solution and illuminated with an LED light source (Figure 1a). SEM images (Figure 1b, Figure S1) reveal the formation of 25 nm thick plate-like structures, many of which have a chiral character. The intersection of growth fronts from adjacent plates does, however, lead to one plate growing over the other where a clear boundary between the two Au structures remains visible. A comparison of the in-plane orientation of adjacent nanoplates reveals a high degree of facet alignment, a result attributed to the heteroepitaxial relationship existing between the Au seeds and the sapphire substrate.[43] Interspersed among the nanoplate structures are irregularly shaped three-dimensional structures. The emergence of such structures is consistent with prior work that revealed that a significant percentage of the seeds lack the internal defect structure needed to promote planar growth.[35] Protruding from each of the plates at the seed position is a roundish structure that often juts out from the underlying seed (Figure 1c, red arrow). This structure, which is typically offset from the center of the plate, is completely encircled but where a small gap is often observed around most of the structure (green arrow). Figure 1d shows SEM images of the five most commonly observed structures where the first two are near-identical chiral structures with opposite handedness. With a close inspection revealing equal numbers of the two enantiomers, the synthesis is one that yields a racemic mixture. The third structure, which is infrequently observed, consists of two interlocking spirals. The final two structures, shaped as hexagonal and triangular nanoplates, are achiral, and it is their formation that severely limits the spiral yield.

With pPhCN being the key reagent in the formation of chiral geometries, a comparison of syntheses with and without its inclusion proves informative. A series of samples were, therefore, prepared in which the evolution of the two growth modes were halted at half-hour intervals. In the absence of pPhCN, the seed first evolves into a faceted hexagon and then grows radially outward (Figure 2a). With the seed thickness being approximately the same as the hexagonal nanoplate, it becomes indiscernible from the final structure. In stark contrast, the inclusion of pPhCN leads to a highly anisotropic growth sequence in which a thin plate nucleates at the base of the seed, grows radially as it encircles the seed from both a clockwise and counterclockwise direction, and then, upon intersection, has one growth front rise over the other to form a
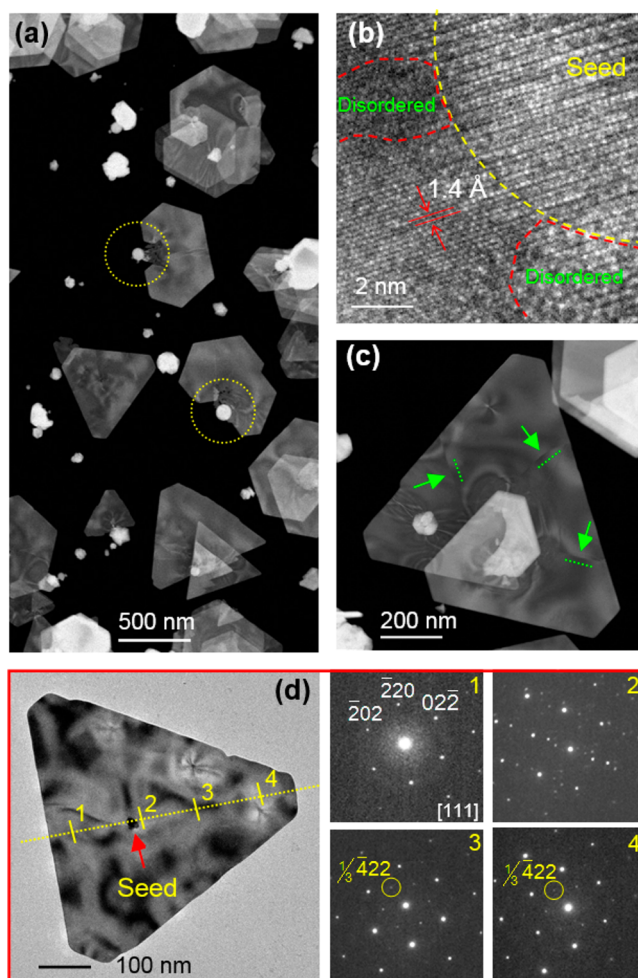

Figure 3. (a) Low-magnification HAADF-STEM image showing early stage spiral growth emanating from the two Au seeds encircled in yellow. (b) High-resolution TEM image of the seed−spiral interface. (c) HAADF-STEM image of a spiral structure with dislocation lines (green). (d) Planar structure and the NBD patterns taken along its length.

spiral arm that then continues to grow (Figure 2b). At the end of the synthesis, the initial seed position is clearly visible and the spiral plate thickness is much less than that of hexagons derived from the pPhCN-free synthesis (Figure S2). With this understanding of the spiral growth mode, it is possible to envision a scenario in which the single spiral growth mode, shown schematically in Figure 2c, could be disrupted by a second nucleation event to yield a double spiral (Figure 2d). The pPhCN growth pathway also differentiates itself in that the first hour of growth is slow but then accelerates to obtain a structure of similar diameter to pPhCN-free synthesis, albeit with significantly less overall volume. A further indication that two-dimensional growth is frustrated in its early stages is that many of the seeds for the 0.5 h pPhCN sample show no indication that a nucleation event has yet occurred (Figure S3). Based on these findings, it is concluded that pPhCN acts to (i) frustrate two-dimensional growth until finally a nucleation event occurs and (ii) prevent the nanoplate from assuming a thickness that is the same as the seed height. It is, however, unlikely that pPhCN is essential to the process that allows one growth front to rise over the other to form a spiral since PVP alone can give rise to such behavior due to the Coulombic
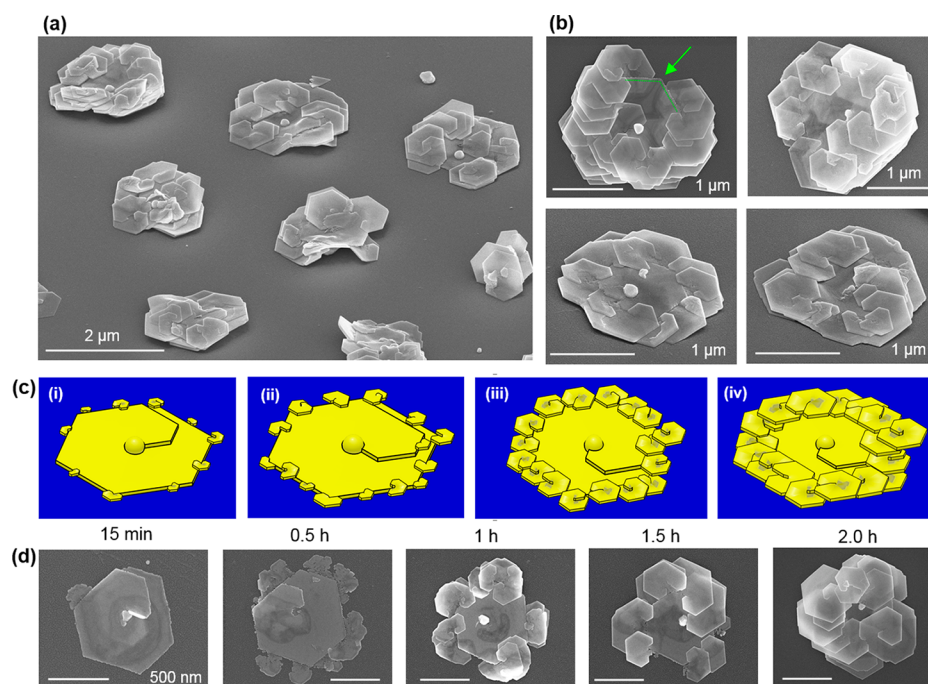
Figure 4. (a) SEM images of hierarchical Au spiral structures derived from a two-step synthesis in which spirals generated in the first step are exposed to fresh reactants. (b) High-magnification images of individual structures taken from both top and tilted views. (c, d) Schematics and SEM images showing the second-step growth progression that occurs over a 2 h interval in which numerous spirals nucleate off the edges of the spiral generated in the first step.

repulsion that occurs when its similarly charged ends approach one another.[27] Instead, by allowing for a highly localized nucleation event off one side of the seed, pPhCN leads to the generation of growth fronts that, once formed, wrap around the seed and collide.

Spiral structures were formed directly on silicon nitride window grids for the purpose of TEM characterization. This necessitated a somewhat inferior method for seed fabrication,[44] yielding Au nanostructures with random placement and a broad size distribution. Nevertheless, individual structures similar to those formed on substrates were readily targeted for investigation. Figure 3a shows a HAADF-STEM image where well-defined seeds have led to early stage spiral growth (circled in yellow). High-resolution images of the seed−spiral attachment point (Figure 3b) show a homoepitaxial connection point but where adjacent areas show a high degree of disorder. The existence of a crystalline point of connection is consistent with the aforementioned observation that adjacent spiral structures on sapphire have their facets aligned since it provides the means by which the seed orientation, as determined by heteroepitaxy at the seed−substrate interface, is imparted to each spiral. Both the seed and the spiral show a (220) interplanar lattice spacing of 1.4 Å, a value consistent with the seed having its [111] orientation normal to the substrate surface. Figure 3c shows an image of an individual spiral exhibiting three dislocation lines (denoted in green) directed toward the central seed, a directionality that is quite common (Figure S4). The variable contrast exhibited by the structure is indicative of a surface that has responded to strain through a slight wrinkling. Figure 3d shows a TEM image of a planar structure and nanobeam electron diffraction (NBD) patterns taken along a line extending from one side of the structure to the other. At all locations, the NBD patterns indicate the presence of the six {220} reflections expected for a

[111]-oriented Au nanoplate. Two of the diffraction patterns show the six weak $^1/_3${422} Au reflections that are nominally forbidden for an fcc crystal structure but which occur when stacking faults run parallel to the (111) basal plane.[45] Such defects are considered essential to the promotion of a planar growth mode.[38,46] Despite these defects, the overall structure shows a high degree of crystallinity where even multiturn spirals express Moiré fringes (Figure S5).

Because the one-pot synthesis resulted in low spiral yields even after carrying out systematic variations to the growth parameters (e.g., reagent concentrations, pH, temperature, illumination conditions), an alternate stepwise synthetic strategy was pursued. Such approaches capitalize on the ease by which substrate-immobilized structures can be inserted and removed from a liquid-state growth solution. They revealed that the chemical environment offered by the one-pot synthesis was one that was rapidly evolving and which only favored certain stages of the spiral growth mode during specific time intervals. When, for example, a seed array is inserted into the growth solution after it has been aged under illumination for 2 h, the ensuing growth proceeds almost as if no pPhCN were present, giving rise to relatively thick planar structures with hexagonal and triangular geometries (Figure S6). Alternatively, if a two-step growth is carried out in which the one-pot synthesis is allowed to proceed in the usual manner to yield structures that are then immersed in fresh reactants, then, instead of perpetuating the first-step growth mode, numerous secondary spirals nucleate and grow off the perimeter of each of the structures formed in the first step. The resulting assemblies, which are shown in Figure 4a,b, were derived from seeds produced using microsphere photolithography (Figure S7)[37] so as to obtain the widely spaced seeds needed for unobstructed growth. The growth mode for these hierarchical assemblies is apparent from the SEM images showing the time
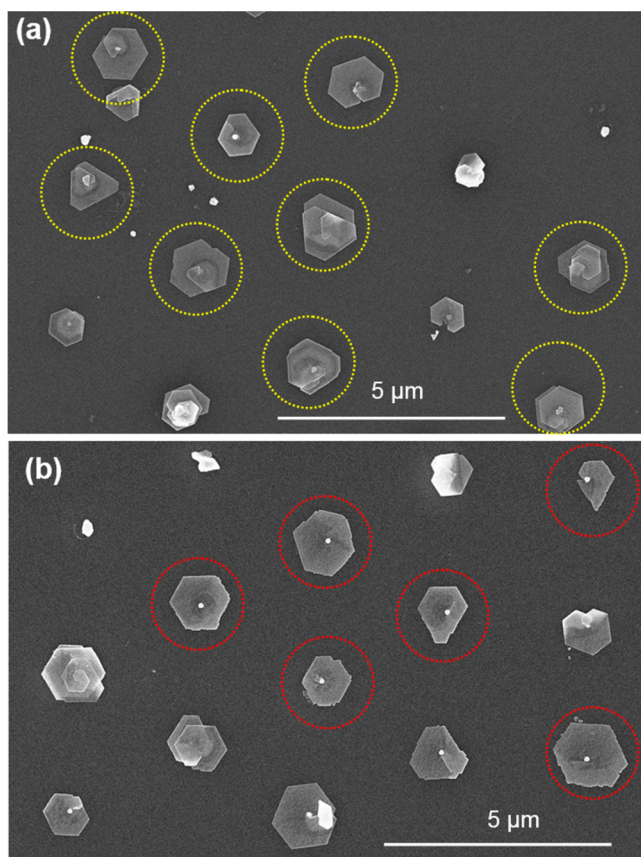
Figure 5. SEM image of an array of Au spirals formed using the (a) optimized two-step synthesis and (b) a one-step synthesis. It should be noted that the two-step procedure yields far more spirals (circled in yellow) while the one-step process often leads to the formation of nanoplates (circled in red).

progression as it relates to the second growth step (Figure 4c,d). It reveals that many nucleation events occur in the first half hour off the edges of the spiral that then evolve into highly faceted spirals. The result shows just how predisposed fresh reactants are to nucleation events that, given the appropriate conditions, can rapidly evolve into spiral morphologies.

With the spiral yield being severely limited by planar growth that encircles the seed but then seamlessly merges to form a hexagonal or triangular nanoplate instead of a chiral structure, it was this merger process that was deemed the synthetic step most detrimental to the spiral growth mode. The synthetic strategy pursued was, therefore, to allow the growth to proceed for the first 75 min in the usual manner to obtain planar structures that encircle the seed but have not yet merged and then transfer them to a second growth solution that provides a chemical environment that is more conducive to a growth front collision process in which one front rises over the other. It was determined that a higher spiral yield occurs when the sample is transferred without rinsing to a second growth solution having a PVP concentration that is one-half that used in the first growth step. Figure 5 shows SEM images comparing the reaction products from the one- and two-step syntheses. Although it may seem somewhat counterintuitive that a reagent known to promote a repulsion when two growth fronts merge[27] can inhibit the same process when oversupplied, it is plausible that excess PVP can lead to its (i) entanglement upon merger or (ii) adsorption to the (111) Au surface in quantities

sufficient to overcome the bending strains needed for one of the growth fronts to lift off the substrate surface.

On the basis of these findings, a three-stage growth mode is forwarded where each stage is dependent on a distinct symmetry-breaking event (for additional details see section S7 of the Supporting Information). In the first stage, Au seeds are submersed in the growth solution, allowing for the attachment of PVP and pPhCN to its surface. With the attachment of PVP to the stacking fault defects being required for this light-driven growth mode to proceed[40] and early stage growth appearing stagnated, it follows that these sites are, in the initial stages, blocked by pPhCN. Over time, however, the effectiveness of pPhCN in blocking these sites becomes increasingly diminished, as is evidenced by the aforementioned growth solution aging experiments. Possible avenues for the deactivation of pPhCN include its consumption through attachment to an ever-increasing number of spontaneously nucleated colloidal Au nanostructures or a light-driven chemical reaction. As pPhCN effectiveness decreases, the attachment of PVP to the Au seeds becomes more probable, a process that eventually triggers a nucleation event at a single point on the perimeter of the seed that favors planar growth. The process, which is in essence a self-regulating ligand-exchange process, provides a break in symmetry to the planar growth mode that would otherwise proceed uniformly about the perimeter of the seed. The second stage is characterized by growth from the site of nucleation whose planar character is dependent on the break in symmetry afforded by the Au stacking faults that run parallel to the substrate surface.[35] The growth proceeds radially outward apart from its encounter with the seed, which acts as an obstacle that must be circumvented. During this stage, the growth is initially slow due to the lingering influences of pPhCN but accelerates as its ability to cap stacking fault defects steadily diminishes, a progression that is accompanied by a transformation in the growth front shape from erratic to highly faceted (Figure 2b). At the same time, the (111) capping of the top facet of the nanoplate remains intact due to the attachment of PVP, pPhCN, or a combination thereof where it is recognized that any role played by pPhCN diminishes over time. The third stage is initiated when the growth fronts encircling the seed collide. At this critical juncture, there is a third symmetry-breaking event that is caused by the Coulombic repulsion occurring when PVP-capped growth fronts collide.[27] This causes one growth front to grow over the other, overcoming any bending strains that arise, and as a result, gives rise to the spiral geometry.

In summary, we have demonstrated a seed-mediated synthesis that is able to generate helical Au spirals at site-specific locations. As a light-driven growth mode, it joins a select list of syntheses in which Au nanostructures having a planar character evolve under illumination.[27,35,40,47−49] The work shows that the spiral growth mode is dependent on sequentially occurring symmetry-breaking events that redirect the growth pathway at critical junctures in the synthesis. By exploiting the ability to rapidly transfer the sample from one growth solution to another, it is possible to further refine the synthesis by exposing the emerging structures to the chemical environment that most efficiently exerts control over specific symmetry-breaking events. In doing so, we have demonstrated a first-of-its-kind substrate-based synthesis while advancing the techniques, strategies, and mechanistic knowhow needed to direct isotropic materials along growth pathways yielding tailored chiral geometries.

■ ASSOCIATED CONTENT

ⓢ Supporting Information

■ AUTHOR INFORMATION

Corresponding Author

Svetlana Neretina − *College of Engineering and Department of Chemistry and Biochemistry, University of Notre Dame, Notre Dame, Indiana 46556, United States;* ⓞ orcid.org/0000-0002-6889-4384; Email: sneretina@nd.edu

Authors

Spencer D. Golze − *College of Engineering, University of Notre Dame, Notre Dame, Indiana 46556, United States*

Stefania Porcu − *Department of Physics, University of Cagliari, 09042 Monserrato (Ca), Italy*

Chen Zhu − *College of Engineering, University of Notre Dame, Notre Dame, Indiana 46556, United States*

Eli Sutter − *Department of Mechanical and Materials Engineering, University of Nebraska-Lincoln, Lincoln, Nebraska 68588, United States;* ⓞ orcid.org/0000-0002-6939-2714

Pier Carlo Ricci − *Department of Physics, University of Cagliari, 09042 Monserrato (Ca), Italy;* ⓞ orcid.org/0000-0001-6191-4613

Edward C. Kinzel − *College of Engineering, University of Notre Dame, Notre Dame, Indiana 46556, United States;* ⓞ orcid.org/0000-0002-4492-8682

Robert A. Hughes − *College of Engineering, University of Notre Dame, Notre Dame, Indiana 46556, United States*

Complete contact information is available at:
https://pubs.acs.org/10.1021/acs.nanolett.0c05105

Notes

The authors declare no competing financial interest.

■ ACKNOWLEDGMENTS

■ REFERENCES

(1) Ma, W.; Xu, L.; de Moura, A. F.; Wu, X.; Kuang, H.; Xu, C.; Kotov, N. A. Chiral Inorganic Nanostructures. *Chem. Rev.* **2017**, *117*, 8041−8093.

(2) Xiao, L.; An, T.; Wang, L.; Xu, X.; Sun, H. Novel Properties and Applications of Chiral Inorganic Nanostructures. *Nano Today* **2020**, *30*, 100824.

(3) Fan, J.; Kotov, N. A. Chiral Nanoceramics. *Adv. Mater.* **2020**, *32*, 1906738.

(4) Kumar, J.; Thomas, K. G.; Liz-Marzan, L. M. Nanoscale Chirality in Metal and Semiconductor Nanoparticles. *Chem. Commun.* **2016**, *52*, 12555−12569.

(5) Urban, M. J.; Shen, C.; Kong, X.-T.; Zhu, C.; Govorov, A. O.; Wang, Q.; Hentschel, M.; Liu, N. Chiral Plasmonic Nanostructures Enabled by Bottom-Up Approaches. *Annu. Rev. Phys. Chem.* **2019**, *70*, 275−299.

(6) Xu, D.; Lin, Q.; Chang, H.-T. Chiral Ag and Au Nanomaterials Based Optical Approaches for Analytical Applications. *Part. Part. Syst. Charact.* **2019**, *36*, 1800552.

(7) Luo, Y.; Chi, C.; Jiang, M.; Li, R.; Zu, S.; Li, Y.; Fang, Z. Plasmonic Chiral Nanostructures: Chiroptical Effects and Applications. *Adv. Opt. Mater.* **2017**, *5*, 1700040.

(8) Valev, V. K.; Baumberg, J. J.; Sibilia, C.; Verbiest, T. Chirality and Chiroptical Effects in Plasmonic Nanostructures: Fundamentals, Recent Progress, and Outlook. *Adv. Mater.* **2013**, *25*, 2517−2534.

(9) Neubrech, F.; Hentschel, M.; Liu, N. Reconfigurable Plasmonic Chirality: Fundamentals and Applications. *Adv. Mater.* **2020**, *32*, 1905640.

(10) Qiu, M.; Zhang, L.; Tang, Z.; Jin, W.; Qiu, C.-W.; Lei, D. Y. 3D Metaphotonic Nanostructures with Intrinsic Chirality. *Adv. Funct. Mater.* **2018**, *28*, 1803147.

(11) Lee, Y. Y.; Kim, R. M.; Im, S. W.; Balamurugan, M.; Nam, K. T. Plasmonic Metamaterials for Chiral Sensing Applications. *Nanoscale* **2020**, *12*, 58−66.

(12) Paiva-Marques, W. A.; Gómez, F. R.; Oliveira, O. N., Jr; Mejía-Salazar, J. R. Chiral Plasmonics and Their Potential for Point-of-Care Biosensing Applications. *Sensors* **2020**, *20*, 944.

(13) Ma, W.; Xu, L.; Wang, L.; Xu, C.; Kuang, H. Chirality-Based Biosensors. *Adv. Funct. Mater.* **2019**, *29*, 1805512.

(14) Hao, C.; Xu, L.; Ma, W.; Wu, X.; Wang, L.; Kuang, H.; Xu, C. Unusual Circularly Polarized Photocatalytic Activity in Nanogapped Gold−Silver Chiroplasmonic Nanostructures. *Adv. Funct. Mater.* **2015**, *25*, 5816−5822.

(15) Liu, T.; Besteiro, L. V.; Liedl, T.; Correa-Duarte, M. A.; Wang, Z.; Govorov, A. O. Chiral Plasmonic Nanocrystals for Generation of Hot Electrons: Toward Polarization-Sensitive Photochemistry. *Nano Lett.* **2019**, *19*, 1395−1407.

(16) Tseng, M. L.; Lin, Z. H.; Kuo, H. Y.; Huang, T. T.; Huang, Y. T.; Chung, T. L.; Chu, C. H.; Huang, J. S.; Tsai, D. P. Stress-Induced 3D Chiral Fractal Metasurface for Enhanced and Stabilized Broadband Near-Field Optical Chirality. *Adv. Opt. Mater.* **2019**, *7*, 1900617.

(17) Zhang, S.; Zhou, J.; Park, Y. S.; Rho, J.; Singh, R.; Nam, S.; Azad, A. K.; Chen, H. T.; Yin, X.; Taylor, A. J.; Zhang, X. Photoinduced Handedness Switching in Terahertz Chiral Metamolecules. *Nat. Commun.* **2012**, *3*, 942.

(18) Soukoulis, C. M.; Wegener, M. Past Achievements and Future Challenges in the Development of Three-Dimensional Photonic Metamaterials. *Nat. Photonics* **2011**, *5*, 523−530.

(19) Mark, A. G.; Gibbs, J. G.; Lee, T.-C.; Fischer, P. Hybrid Nanocolloids with Programmed Three-Dimensional Shape and Material Composition. *Nat. Mater.* **2013**, *12*, 802−807.

(20) Liu, J.; Ni, Z.; Nandi, P.; Mirsaidov, U.; Huang, Z. Chirality Transfer in Galvanic Replacement Reactions. *Nano Lett.* **2019**, *19*, 7427−7433.

(21) Zhang, M.; Pacheco-Peña, V.; Yu, Y.; Chen, W.; Greybush, N. J.; Stein, A.; Engheta, N.; Murray, C. B.; Kagan, C. R. Nanoimprinted Chiral Plasmonic Substrates with Three-Dimensional Nanostructures. *Nano Lett.* **2018**, *18*, 7389−7394.

(22) Goerlitzer, E. S. A.; Mohammadi, R.; Nechayev, S.; Banzer, P.; Vogel, N. Large-Area 3D Plasmonic Crescents with Tunable Chirality. *Adv. Optical Mater.* **2019**, *7*, 180177.

(23) Shukla, N.; Gellman, A. J. Chiral Metal Surfaces for Enantioselective Processes. *Nat. Mater.* **2020**, *19*, 939−945.

(24) Song, C.; Blaber, M. G.; Zhao, G.; Zhang, P.; Fry, H. C.; Schatz, G. C.; Rosi, N. L. Tailorable Plasmonic Circular Dichroism Properties of Helical Nanoparticle Superstructure. *Nano Lett.* **2013**, *13*, 3256−3261.

(25) Zhou, C.; Duan, X.; Liu, N. DNA-Nanotechnology-Enabled Chiral Plasmonics: From Static to Dynamic. *Acc. Chem. Res.* **2017**, *50*, 2906−2914.

(26) Lee, H.-E.; Ahn, H.-Y.; Mun, J.; Lee, Y. Y.; Kim, M.; Cho, N. H.; Chang, K.; Kim, W. S.; Rho, J.; Nam, K. T. Amino-Acid- and Peptide-Directed Synthesis of Chiral Plasmonic Gold Nanoparticles. *Nature* **2018**, *556*, 360−365.

(27) Zhai, Y.; Zhang, F.; Zhang, B.; Gao, X. Engineering Single Nanopores on Gold Nanoplates by Tuning Crystal Screw Dislocation. *Adv. Mater.* **2017**, *29*, 1703102.

(28) Morin, S. A.; Forticaux, A.; Bierman, M. J.; Jin, S. Screw Dislocation-Driven Growth of Two-Dimensional Nanoplates. *Nano Lett.* **2011**, *11*, 4449−4455.

(29) Jang, M. H.; Kim, J. K.; Tak, H.; Yoo, H. Controllable Synthesis of Multi-Layered Gold Spirangles. *J. Mater. Chem.* **2011**, *21*, 17606−17608.

(30) Suito, E.; Uyeda, N. Electron Microscopy and Diffraction Studies on the Growth and Structure of Laminar Single Crystals of Colloidal Gold. *Bull. Inst. Chem. Res., Kyoto Univ.* **1965**, *42*, 511−541.

(31) Chiang, Y.; Turkevich, J. Formation of Platelike Colloidal Gold. *J. Colloid Sci.* **1963**, *18*, 772−783.

(32) Knoppe, S.; Burgi, T. Chirality in Thiolate-Protected Gold Clusters. *Acc. Chem. Res.* **2014**, *47*, 1318−1326.

(33) Kim, J.-Y.; Yeom, J.; Zhao, G.; Calcaterra, H.; Munn, J.; Zhang, P.; Kotov, N. Assembly of Gold Nanoparticles into Chiral Superstructures Driven by Circularly Polarized Light. *J. Am. Chem. Soc.* **2019**, *141*, 11739−11744.

(34) Morisawa, K.; Ishida, T.; Tatsuma, T. Photoinduced Chirality Switching of Metal-Inorganic Plasmonic Nanostructures. *ACS Nano* **2020**, *14*, 3603−3609.

(35) Golze, S. D.; Hughes, R. A.; Rouvimov, S.; Neal, R. D.; Demille, T. B.; Neretina, S. Plasmon-Mediated Synthesis of Periodic Arrays of Gold Nanoplates using Substrate-Immobilized Seeds Lined with Planar Defects. *Nano Lett.* **2019**, *19*, 5653−5660.

(36) Menumerov, E.; Golze, S. D.; Hughes, R. A.; Neretina, S. Arrays of Highly Complex Noble Metal Nanostructures using Nanoimprint Lithography in Combination with Liquid-Phase Epitaxy. *Nanoscale* **2018**, *10*, 18186−18194.

(37) Qu, C.; Kinzel, E. C. Polycrystalline Metasurface Perfect Absorbers Fabricated Using Microsphere Photolithography. *Opt. Lett.* **2016**, *41*, 3399−3402.

(38) Tan, T.; Zhang, S.; Wang, J.; Zheng, Y.; Lai, H.; Liu, J.; Qin, F.; Wang, C. Resolving the Stacking Fault Structure of Silver Nanoplates. *Nanoscale* **2021**, *13*, 195−205.

(39) Langille, M. R.; Personick, M. L.; Mirkin, C. A. Plasmon-Mediated Syntheses of Metallic Nanostructures. *Angew. Chem., Int. Ed.* **2013**, *52*, 13910−13940.

(40) Zhai, Y.; DuChene, J. S.; Wang, Y.-C.; Qiu, J.; Johnston-Peck, A. C.; You, B.; Guo, W.; DiCiaccio, B.; Qian, K.; Zhao, E. W.; Ooi, F.; Hu, D.; Su, D.; Stach, E. A.; Zhu, Z.; Wei, W. D. Polyvinylpyrrolidone-Induced Anisotropic Growth of Gold Nanoprisms in Plasmon-Driven Synthesis. *Nat. Mater.* **2016**, *15*, 889−893.

(41) Porcu, S.; Castellino, M.; Roppolo, I.; Carbonaro, C. M.; Palmas, S.; Mais, L.; Casula, M. F.; Neretina, S.; Hughes, R. A.; Secci, F.; Ricci, P. C. Highly Efficient Visible Light Phenyl Modified Carbon Nitride/TiO₂ Photocatalyst for Environmental Applications. *Appl. Surf. Sci.* **2020**, *531*, 147394.

(42) Porcu, S.; Roppolo, I.; Salaun, M.; Sarais, G.; Barbarossa, S.; Casula, M. F.; Carbonaro, C. M.; Ricci, P. C. Come to Light: Detailed Analysis of Thermally Treated Phenyl Modified Carbon Nitride Polymorphs for Bright Phosphors in Lighting Applications. *Appl. Surf. Sci.* **2020**, *504*, 144330.

(43) Hajfathalian, M.; Gilroy, K. D.; Hughes, R. A.; Neretina, S. Citrate−Induced Nanocubes: A Reexamination of the Role of Citrate as a Shape−Directing Capping Agent for Ag-Based Nanostructures. *Small* **2016**, *12*, 3444−3452.

(44) Farzinpour, P.; Sundar, A.; Gilroy, K. D.; Eskin, Z. E.; Hughes, R. A.; Neretina, S. Altering the Dewetting Characteristics of Ultrathin Gold and Silver Films using a Sacrificial Antimony Layer. *Nanotechnology* **2012**, *23*, 495604.

(45) Germain, V.; Li, J.; Ingert, D.; Wang, Z. L.; Pileni, M. P. Stacking Faults in Formation of Silver Nanodisks. *J. Phys. Chem. B* **2003**, *107*, 8717−8720.

(46) Xia, Y.; Gilroy, K. D.; Peng, H. C.; Xia, X. Seed-Mediated Growth of Colloidal Metal Nanocrystals. *Angew. Chem., Int. Ed.* **2017**, *56*, 60−95.

(47) Tangeysh, B.; Tibbetts, K. M.; Odhner, J. H.; Wayland, B. B.; Levis, R. J. Triangular Gold Nanoplate Growth by Oriented Attachment of Au Seeds Generated by Strong Field Laser Reduction. *Nano Lett.* **2015**, *15*, 3377−3382.

(48) Guo, W.; Johnston-Peck, A.; Zhang, Y.; Hu, Y.; Huang, J.; Wei, W. D. Cooperation of Hot Holes and Surface Adsorbates in Plasmon-Driven Anisotropic Growth of Gold Nanostars. *J. Am. Chem. Soc.* **2020**, *142*, 10921−10925.

(49) Long, Y.; Wang, S.; Wang, Y.; Qiao, Y.; Ding, T. Light-Directed On-Chip Shape Transformation of a Single Gold Nanoparticle. *J. Mater. Chem. C* **2020**, *8*, 16198−16203.